


Measuring Spin of the Remnant Black Hole from Maximum Amplitude

Deborah Ferguson¹,[✉] Sudarshan Ghonge,¹ James A. Clark,¹ Juan Calderon Bustillo,^{2,3}
Pablo Laguna,¹ and Deirdre Shoemaker¹

¹*Center for Relativistic Astrophysics and School of Physics, Georgia Institute of Technology, Atlanta, Georgia 30332, USA*

²*Monash Centre for Astrophysics, School of Physics and Astronomy, Monash University, VIC 3800, Australia*

³*OzGrav: The ARC Centre of Excellence for Gravitational-Wave Discovery, Clayton, VIC 3800, Australia*

 (Received 10 May 2019; revised manuscript received 27 June 2019; published 8 October 2019)

Gravitational waves emitted during the merger of two black holes carry information about the remnant black hole, namely its mass and spin. This information is typically found from the ringdown radiation as the black hole settles to a final state. We find that the remnant black hole spin is already known at the peak amplitude of the gravitational wave strain. Using this knowledge, we present a new method for measuring the final spin that is template independent, using only the chirp mass, the instantaneous frequency of the strain, and its derivative at maximum amplitude, all template independent.

DOI: 10.1103/PhysRevLett.123.151101

Introduction.—The advent of gravitational wave (GW) astronomy has granted us the opportunity to observationally study compact binary coalescences. During the course of the first two observing runs, LIGO [1] and Virgo [2] detected GWs from a total of ten coalescing binary black holes (BBHs) and one binary neutron star [3,4]. These systems have hinted at the population properties of BBHs such as the distributions of mass, spin and redshifts [5], and have placed GW observations into the new era of multi-messenger astronomy [4,6].

In the few years since the first detection of GWs [7], we have learned a tremendous amount about the parameter space of stellar-mass black holes (BHs) [5]. Each stage of the coalescence provides information about the BBH system; this study focuses on the parameters describing the remnant BH. The product of a BBH merger is a perturbed BH that emits ringdown radiation as it settles to a Kerr BH. This process provides fundamental information to understand gravity in its most extreme regime. Perturbation theory tells a compelling story about how perturbed BHs, like the remnant of a BBH merger, lose the information about the disturbance, often called hair, in the form of GWs [8]. Perturbed BHs ring down or emit GWs with a frequency (ω_{QNM}) and decay time (τ_{QNM}) characterized by the BH mass and spin [9], providing the means to determine the remnant BH parameters upon the detection of GWs.

The GW during this ringdown phase is generally represented as the sum of quasinormal modes, each expressible as a damped sinusoid with its own ω_{QNM} and τ_{QNM} , fixed by the mass and spin of the final BH [10–12]. The Echeverria formulas [13] provide relationships to determine the BH mass and spin from ω_{QNM} and τ_{QNM} using spheroidal harmonics.

There have been attempts to measure ω_{QNM} and τ_{QNM} of the ringdown [14–20] and as the detectors improve in

sensitivity, this will become more viable. One commonly considered method is to estimate the ringdown parameters by matching directly to the exponentially decaying ringdown, where Ref. [17] finds consistent results for GW150914 searching for damped sinusoids. The possibility of using GWs to detect this spectrum of radiation is often referred to as BH spectroscopy [21–23]. The short duration and low amplitude of the signal expected from stellar-mass mergers, however, makes this postmerger phase challenging to detect, which is further compounded by the reliance upon knowing when ringdown begins [24,25].

Because of these challenges, current approaches [26–28] to estimate the spin of the final BH match the data to theoretical models of the inspiral. Fortunately, numerical relativity (NR) provides the map from initial to final parameters [29–31] that are used to estimate the final spin. For systems with many cycles of inspiral, this method can predict the remnant spin with precision, assuming general relativity (GR). It is desirable to obtain the remnant spin independently of matched filtering of either the inspiral or ringdown in order to perform tests of GR [26,32–34]. One can also perform tests of GR directly from the peak frequency [35].

With the goal of avoiding the use of the exponentially decaying ringdown, we propose a method of determining the final spin that takes advantage of the higher amplitude at the merger of two BHs. The method proposed here builds on earlier work by Healy *et al.* [36] which connected the instantaneous frequency of the GW at peak amplitude to ω_{QNM} and τ_{QNM} of the ringdown. While it is not obvious that such a relationship should exist, there have been hints of the merged black hole entering a perturbative regime as early as the peak amplitude [36–39] with the radiation near the peak amplitude of the strain being described by quasinormal modes that include the overtones. In this

Letter, we find that the spin of the remnant black hole is already known at the peak amplitude.

Inspired by the results of Healy *et al.*, we create a map linking the instantaneous frequency at maximum amplitude (ω_{peak}), the derivative of the instantaneous frequency at maximum amplitude ($\dot{\omega}_{\text{peak}}$), and the chirp mass (\mathcal{M}) to the dimensionless remnant spin (a_f). One advantage of this method is that all measurements involved, ω_{peak} , $\dot{\omega}_{\text{peak}}$, and \mathcal{M} , are independent of fitting the data to a model waveform. Furthermore, \mathcal{M} has the advantage of needing only a few prepeak cycles to obtain a good measurement using a well-known gravitational-wave algorithm, Coherent WaveBurst (CWB) [40]. In the following we (a) demonstrate a tight relation between the frequency properties measured at peak and the spin of the final BH and (b) develop an algorithm to exploit this relationship on GW observations.

In the Methodology section, we describe the NR data used to derive a connection from ω_{peak} , $\dot{\omega}_{\text{peak}}$, \mathcal{M} to a_f and discuss the associated errors. In the Final Spin section, we examine the viability of the relationship as a form of parameter estimation with noisy data. Finally, we summarize our findings in the Conclusions section.

Methodology.—NR Catalog and Errors: The relationships found in this Letter are based upon the use of 112 NR simulations provided by the Georgia Tech waveform catalog, 47 of which are nonspinning and 65 of which are aligned spin, with mass ratios $1 < q < 10$ [41]. The Georgia Tech waveforms are produced using the MAYA code [42–45], a branch of the Einstein Toolkit [46], a NR code built upon Cactus with mesh refinement from Carpet [47] with the addition of thorns to calculate various quantities during the simulation including an apparent horizon solver [48].

We create a map from ω_{peak} , $\dot{\omega}_{\text{peak}}$, \mathcal{M} to a_f . As will be described in subsection “Fitting to final spin,” this equates to a mapping from the dimensionless instantaneous frequency at maximum amplitude ($\hat{\omega}_{\text{peak}}$), the derivative of the dimensionless instantaneous frequency at maximum amplitude ($\hat{\dot{\omega}}_{\text{peak}}$), and the symmetric mass ratio (η) to a_f .

In order to create this mapping, $\hat{\omega}_{\text{peak}}$, $\hat{\dot{\omega}}_{\text{peak}}$, and a_f are obtained from the NR simulation data. In this Letter we use the strain $h(t)$ for ease of working with the GW detectors, given

$$h(t) = h_+(t) - ih_\times(t) = \int_{-\infty}^t dt' \int_{-\infty}^{t'} dt'' \psi_4(t''),$$

and computed according to [49]. Strain is represented as a sum of spin-weighted spherical harmonics ${}_{-2}Y_{\ell,m}$ given by

$$h(t, \theta, \phi) = \sum_{\ell,m} {}_{-2}Y_{\ell,m}(\theta, \phi) h_{\ell,m}(t),$$

where $h_{\ell,m}$ are excited depending on the inspiral parameters and the binary’s orientation with respect to the

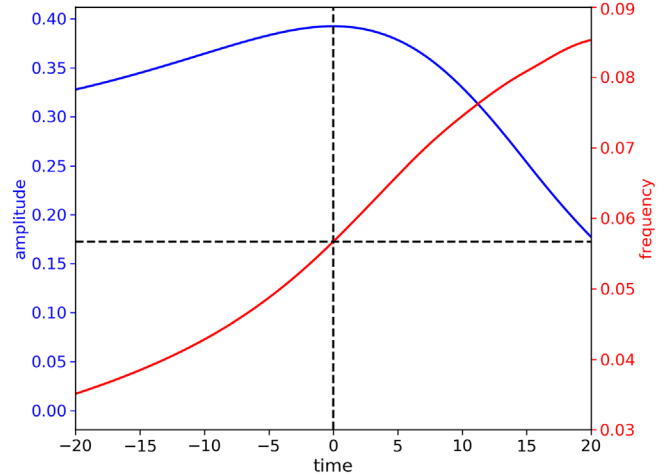


FIG. 1. The figure depicts the amplitude and the frequency during merger. The vertical dotted line denotes the time of maximum amplitude and the horizontal dotted line shows the corresponding instantaneous frequency.

observer. In aligned spin scenarios and face on orientations, the $\ell = 2$, $m = 2$ mode dominates the signal, and, therefore, this study uses only the $\ell = 2$, $m = 2$ mode [50–53].

The GW amplitude is thus $|h_{22}(t)|$, and the instantaneous frequency is found as the derivative of the phase, i.e., $\dot{\phi}(t)$ where $\phi(t) = \arg[h_{22}(t)]$. $\hat{\omega}_{\text{peak}}$ and $\hat{\dot{\omega}}_{\text{peak}}$ are obtained simply by identifying the time at which the amplitude reaches a maximum and grabbing the instantaneous frequency and its time derivative at that time. This is shown visually in Fig. 1. Note a_f is determined from the apparent horizon of the remnant BH.

The finite spatial and temporal resolutions of NR simulations introduce systematic uncertainty into the estimates of frequency and spin. By repeating each simulation at multiple resolutions, the error is found to be of the order of 0.01% for a_f , 1% for $\hat{\omega}_{\text{peak}}$, and 1.4% for $\hat{\dot{\omega}}_{\text{peak}}$. These uncertainties account for the spread in the fit shown in Fig. 2.

Fitting to final spin: With the data selected and the NR errors understood, we can create a fit that connects the peak amplitude of GW strain to the final BH spin. In order to create this fitting from ω_{peak} , $\dot{\omega}_{\text{peak}}$, and \mathcal{M} to a_f using NR simulations, we utilize the following relationships:

$$\hat{\omega}\eta^{3/5} = \omega\mathcal{M}, \quad (1)$$

$$\hat{\dot{\omega}}\eta^{6/5} = \dot{\omega}\mathcal{M}^2, \quad (2)$$

where η is the symmetric mass ratio defined as a function of the initial masses m_1 and m_2 :

$$\eta = \frac{m_1 m_2}{(m_1 + m_2)^2}, \quad (3)$$

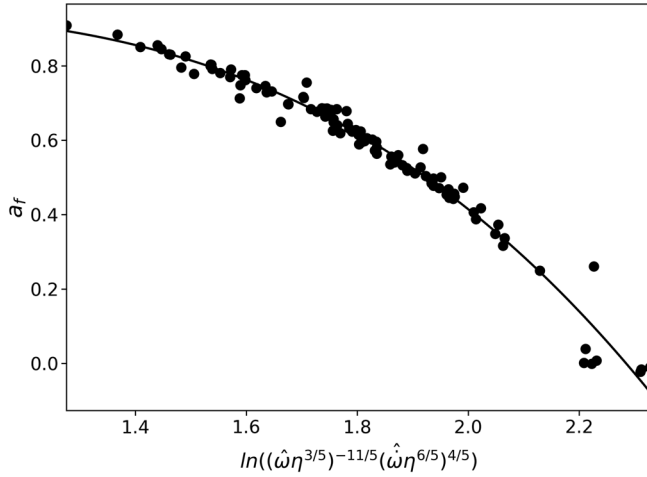


FIG. 2. We plot the dimensionless spin of the remnant black hole versus a function of symmetric mass ratio, instantaneous dimensionless frequency, and its time derivative at maximum strain for aligned spin numerical relativity waveforms. The solid line shows the fitting relation described in the “Fitting to final spin” subsection.

and \mathcal{M} is the chirp mass expressible as

$$\mathcal{M} = \eta^{3/5} M = \frac{c^3}{G} \left(\frac{5}{96} \pi^{-8/3} f^{-11/3} \dot{f} \right)^{3/5}. \quad (4)$$

These lead us to plot the spin of the remnant BH against a function of $\hat{\omega}_{\text{peak}} \eta^{3/5}$ and $\hat{\omega}_{\text{peak}} \eta^{6/5}$ which will take the form

$$x = \ln[(\hat{\omega}_{\text{peak}} \eta^{3/5})^{-11/5} (\hat{\omega}_{\text{peak}} \eta^{6/5})^{4/5}]. \quad (5)$$

The resulting fit is shown in Fig 2. Adopting the same functional form as Healy *et al.* [36], we obtain the following best fit relationship:

$$a_f = -0.216x^3 + 0.415x^2 - 0.252x + 0.989, \quad (6)$$

with an average spread of $\Delta a_f = 0.032$.

Final spin.—Having found an NR derived relationship relating ω_{peak} , $\dot{\omega}_{\text{peak}}$, and \mathcal{M} to a_f , it is important to study how these values are obtained from real data and how precise this method will be when faced with a detection. \mathcal{M} is measured by burst searches that fit the frequency evolution of the signal [40]. By analyzing the recovered \mathcal{M} of existing CWB runs, and using the knowledge that the uncertainty scales as $1/\text{signal-to-noise ratio (SNR)}$ [54], we estimate that the uncertainty in \mathcal{M} as recovered by CWB is $\sim 1.5/\text{SNR}$. This contributes an additional uncertainty of $(126/\text{SNR})\%$ to a_f . For the $\text{SNR} = 100$ runs we analyze in this Letter, this adds an uncertainty of 1.26% to a_f .

Since GW detector data are noisy, we cannot reliably obtain ω_{peak} and $\dot{\omega}_{\text{peak}}$ directly without first denoising it. In order to reconstruct a signal out of the noise, we use BayesWave, a search pipeline that relies on modeling the

GW as a number of sine Gaussians whose sum results in a coherent GW signal in a detector network [55]. By using this morphology-agnostic approach, the reconstructed waveform is robust against uncertainties which may be present in templated analyses. The latter, often referred to as CBC analyses, model the waveform based on the time orbital evolution of compact binary coalescences [56]. BayesWave provides an independent, complementary estimate of the waveform morphology, and consequently avoids systematic uncertainty in the frequency evolution which might be present in the best fit CBC waveform [57,58]. In this study we analyze the waveform as reconstructed by BayesWave for the Livingston detector only.

To quantify the expected uncertainty in the remnant spin, we performed a systematic Monte Carlo study whereby sets of BBH signals with increasing SNR [59] were added to stationary Gaussian noise colored with the power spectral density of O1 era LIGO detectors. The underlying waveforms for these “injections” were then recovered using BayesWave. For a SNR of 100, we injected a h_{22} signal consistent with that of GW150914 in 2000 realizations of Gaussian noise and recovered ω_{peak} and $\dot{\omega}_{\text{peak}}$ for the median waveform of each. The value of ω_{peak} was obtained by first calculating the amplitude envelope of the median whitened waveform (using a PYTHON implementation of the Hilbert-Huang transform [60]) and then locating the time at which the amplitude is maximum. Then the median time frequency track, outputted by BayesWave, is used to identify the frequency and the time derivative of the frequency at the given time.

Figure 3 shows the cumulative probability distribution of the estimated a_f for our 2000 injections. The solid black line denotes the median, the solid red line denotes the true

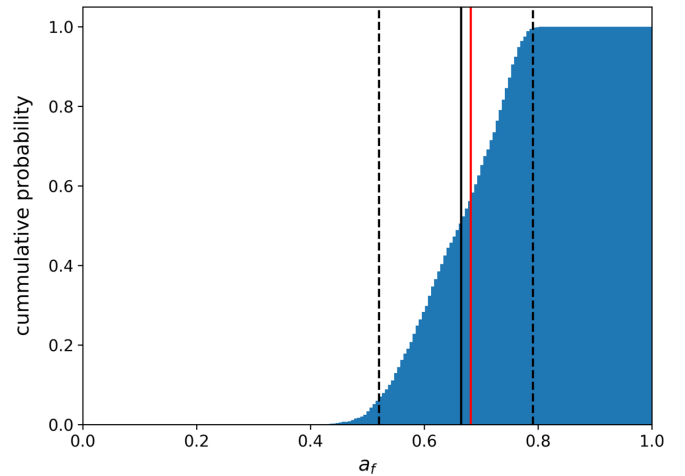


FIG. 3. We plot the cumulative probability distribution of the final dimensionless spin obtained for a GW150914-like signal injected into noise and recovered using BayesWave with SNR 100. The solid black line shows the median recovered spin and the dotted black lines show the 90% confidence interval. The solid red line shows the true spin.

TABLE I. Median and 90% confidence values of a_f for various SNRs.

SNR	Median	Lower 90% confidence	Upper 90% confidence
40	0.671	0.437	0.802
60	0.677	0.484	0.785
80	0.654	0.497	0.782
100	0.667	0.510	0.772

final spin, and the dotted lines show the 90% confidence interval, which is $a_f = (0.51, 0.77)$ for SNR of 100.

To better understand how this error scales with SNR, we used the same technique just described with 250 injections each for SNRs 40, 60, 80, and 100. The resulting medians and 90% confidence intervals are shown in Table I.

Conclusions.—This study finds that the remnant spin is known at the peak amplitude and presents a method of estimating it from the chirp mass, the frequency at maximum amplitude of the strain, and its derivative in an analytic relationship. This allows us to make use of the high SNR at the peak to estimate the final spin before entering the perturbative ringdown regime.

In order to understand the viability of this study as a parameter estimation method, we analyzed the distribution of the remnant spin obtained via recovering the waveform of a GW150914-like signal with increasing SNRs from 40 to 100. We demonstrate that we can reliably place bounds on the spin of the remnant BH using information found near the peak amplitude when the signal is dominated by the $\ell = 2$, $m = 2$ mode.

Our method avoids the usage of BBH templates, instead obtaining ω_{peak} and $\dot{\omega}_{\text{peak}}$ from a BayesWave reconstruction and \mathcal{M} from CWB. While matched filtering methods likely place a tighter bound on the remnant spin, our alternate approach is not subject to the same systematic biases due to waveform modeling present in the matched filter search. There remain systematic errors due to the fit we are using to determine the final spin from the peak amplitude. In addition, the fitting formula is an interpolation over a discrete set of NR templates and might change if more NR simulations are added to the fit.

The next steps in this study will see the method applied to all the LIGO/VIRGO BBH detections with reasonable BayesWave reconstructions from O1, O2, and, soon, O3. It will also be interesting to see the effect of adding precessing runs to the fit and whether this analysis can be expanded to include higher modes.

P. L. and D. S. gratefully acknowledge support from the NSF Grants No. PHY-1806580, No. PHY-1809572, No. PHY-1550461, and No. 1333360, XSEDE TG-PHY120016. J. C. B. also acknowledges support from Australian Research Council Discovery Project No. DP180103155. This research was also supported in

part through research cyberinfrastructure resources and services provided by the Partnership for an Advanced Computing Environment (PACE) at the Georgia Institute of Technology. The authors are grateful for computational resources provided by the LIGO Laboratory and supported by National Science Foundation Grants No. PHY-0757058 and No. PHY-0823459. We also thank Karan Jani for useful discussions.

- [1] J. Aasi *et al.* (LIGO Scientific Collaboration), *Classical Quantum Gravity* **32**, 074001 (2015).
- [2] F. Acernese *et al.* (Virgo Collaboration), *Classical Quantum Gravity* **32**, 024001 (2015).
- [3] LIGO Scientific and Virgo Collaborations, *Phys. Rev. X* **9**, 031040 (2019).
- [4] LIGO Scientific and Virgo Collaborations, *Phys. Rev. Lett.* **119**, 161101 (2017).
- [5] LIGO Scientific and Virgo Collaborations, [arXiv: 1811.12940](https://arxiv.org/abs/1811.12940).
- [6] P. Ma sz ros, D. B. Fox, C. Hanna, and K. Murase, [arXiv: 1906.10212](https://arxiv.org/abs/1906.10212).
- [7] LIGO Scientific and Virgo Collaborations, *Phys. Rev. Lett.* **116**, 061102 (2016).
- [8] C. V. Vishveshwara, *Phys. Rev. D* **1**, 2870 (1970).
- [9] W. H. Press, *Astrophys. J. Lett.* **170**, L105 (1971).
- [10] H.-P. Nollert and R. H. Price, *J. Math. Phys. (N.Y.)* **40**, 980 (1999).
- [11] K. D. Kokkotas and B. G. Schmidt, *Living Rev. Relativity* **2**, 2 (1999).
- [12] E. Berti, V. Cardoso, and A. O. Starinets, *Classical Quantum Gravity* **26**, 163001 (2009).
- [13] F. Echeverria, *Phys. Rev. D* **40**, 3194 (1989).
- [14] B. P. Abbott *et al.* (LIGO Scientific Collaboration), *Phys. Rev. D* **80**, 062001 (2009).
- [15] L. M. Goggin (LIGO Scientific Collaboration), *Classical Quantum Gravity* **23**, S709 (2006).
- [16] E. Berti, J. Cardoso, V. Cardoso, and M. Cavaglia, *Phys. Rev. D* **76**, 104044 (2007).
- [17] G. Carullo, W. Del Pozzo, and J. Veitch, *Phys. Rev. D* **99**, 123029 (2019).
- [18] H. Yang, K. Yagi, J. Blackman, L. Lehner, V. Paschalidis, F. Pretorius, and N. Yunes, *Phys. Rev. Lett.* **118**, 161101 (2017).
- [19] H. Nakano, T. Narikawa, K.-i. Oohara, K. Sakai, H.-a. Shinkai, H. Takahashi, T. Tanaka, N. Uchikata, S. Yamamoto, and T. S. Yamamoto, *Phys. Rev. D* **99**, 124032 (2019).
- [20] M. Cabero, C. D. Capano, O. Fischer-Birnholtz, B. Krishnan, A. B. Nielsen, A. H. Nitz, and C. M. Biwer, *Phys. Rev. D* **97**, 124069 (2018).
- [21] O. Dreyer, B. J. Kelly, B. Krishnan, L. S. Finn, D. Garrison, and R. Lopez-Aleman, *Classical Quantum Gravity* **21**, 787 (2004).
- [22] E. Berti, V. Cardoso, and C. M. Will, *Phys. Rev. D* **73**, 064030 (2006).
- [23] R. Brito, A. Buonanno, and V. Raymond, *Phys. Rev. D* **98**, 084038 (2018).

- [24] S. Bhagwat, M. Okounkova, S. W. Ballmer, D. A. Brown, M. Giesler, M. A. Scheel, and S. A. Teukolsky, *Phys. Rev. D* **97**, 104065 (2018).
- [25] G. Carullo, L. van der Schaaf, L. London, P. T. H. Pang, K. W. Tsang, O. A. Hannuksela, J. Meidam, M. Agathos, A. Samajdar, A. Ghosh, T. G. F. Li, W. Del Pozzo, and C. Van Den Broeck, *Phys. Rev. D* **98**, 104020 (2018).
- [26] B. P. Abbott *et al.* (Virgo and LIGO Scientific Collaborations), *Phys. Rev. Lett.* **116**, 221101 (2016); **121**, 129902(E) (2018).
- [27] J. Healy, C. O. Lousto, and Y. Zlochower, *Phys. Rev. D* **90**, 104004 (2014).
- [28] L. Rezzolla, P. Diener, E. N. Dorband, D. Pollney, C. Reisswig, E. Schnetter, and J. Seiler, *Astrophys. J.* **674**, L29 (2008).
- [29] J. Healy and C. O. Lousto, *Phys. Rev. D* **95**, 024037 (2017).
- [30] X. Jiménez-Forteza, D. Keitel, S. Husa, M. Hannam, S. Khan, and M. Pürrer, *Phys. Rev. D* **95**, 064024 (2017).
- [31] F. Hofmann, E. Barausse, and L. Rezzolla, *Astrophys. J. Lett.* **825**, L19 (2016).
- [32] B. P. Abbott *et al.* (LIGO Scientific and Virgo Collaborations), [arXiv:1903.04467](https://arxiv.org/abs/1903.04467).
- [33] A. Ghosh, N. K. Johnson-McDaniel, A. Ghosh, C. K. Mishra, P. Ajith, W. Del Pozzo, C. P. L. Berry, A. B. Nielsen, and L. London, *Classical Quantum Gravity* **35**, 014002 (2018).
- [34] A. Ghosh *et al.*, *Phys. Rev. D* **94**, 021101(R) (2016).
- [35] G. Carullo, G. Riemenschneider, K. W. Tsang, A. Nagar, and W. Del Pozzo, *Classical Quantum Gravity* **36**, 105009 (2019).
- [36] J. Healy, P. Laguna, and D. Shoemaker, *Classical Quantum Gravity* **31**, 212001 (2014).
- [37] A. Buonanno, G. B. Cook, and F. Pretorius, *Phys. Rev. D* **75**, 124018 (2007).
- [38] I. Kamaretsos, M. Hannam, and B. S. Sathyaprakash, *Phys. Rev. Lett.* **109**, 141102 (2012).
- [39] M. Giesler, M. Isi, M. Scheel, and S. Teukolsky, [arXiv:1903.08284](https://arxiv.org/abs/1903.08284).
- [40] V. Tiwari, S. Klimentko, V. Nacula, and G. Mitselmakher, *Classical Quantum Gravity* **33**, 01LT01 (2016).
- [41] K. Jani, J. Healy, J. A. Clark, L. London, P. Laguna, and D. Shoemaker, *Classical Quantum Gravity* **33**, 204001 (2016).
- [42] F. Herrmann, I. Hinder, D. Shoemaker, and P. Laguna, *Classical Quantum Gravity* **24**, S33 (2007).
- [43] B. Vaishnav, I. Hinder, F. Herrmann, and D. Shoemaker, *Phys. Rev. D* **76**, 084020 (2007).
- [44] J. Healy, J. Levin, and D. Shoemaker, *Phys. Rev. Lett.* **103**, 131101 (2009).
- [45] L. Pekowsky, R. O’Shaughnessy, J. Healy, and D. Shoemaker, *Phys. Rev. D* **88**, 024040 (2013).
- [46] F. Löffler *et al.*, *Classical Quantum Gravity* **29**, 115001 (2012).
- [47] E. Schnetter, S. H. Hawley, and I. Hawke, *Classical Quantum Gravity* **21**, 1465 (2004).
- [48] J. Thornburg, *Classical Quantum Gravity* **21**, 743 (2004).
- [49] C. Reisswig and D. Pollney, *Classical Quantum Gravity* **28**, 195015 (2011).
- [50] J. Calderon Bustillo, P. Laguna, and D. Shoemaker, *Phys. Rev. D* **95**, 104038 (2017).
- [51] J. Calderon Bustillo, S. Husa, A. M. Sintes, and M. Prer, *Phys. Rev. D* **93**, 084019 (2016).
- [52] L. Pekowsky, J. Healy, D. Shoemaker, and P. Laguna, *Phys. Rev. D* **87**, 084008 (2013).
- [53] V. Varma and P. Ajith, *Phys. Rev. D* **96**, 124024 (2017).
- [54] M. Vallisneri, *Phys. Rev. D* **77**, 042001 (2008).
- [55] N. J. Cornish and T. B. Littenberg, *Classical Quantum Gravity* **32**, 135012 (2015).
- [56] S. Fairhurst and P. Brady, *Classical Quantum Gravity* **25**, 105002 (2008).
- [57] J. Veitch, V. Raymond, B. Farr, W. Farr, P. Graff, S. Vitale, B. Aylott, K. Blackburn, N. Christensen, M. Coughlin *et al.*, *Phys. Rev. D* **91**, 042003 (2015).
- [58] C. Messick *et al.*, *Phys. Rev. D* **95**, 042001 (2017).
- [59] E. Parzen, *IEEE Trans. Inf. Theory* **9**, 127 (2006).
- [60] N. E. Huang, Z. Shen, S. R. Long, M. C. Wu, H. H. Shih, Q. Zheng, N.-C. Yen, C. C. Tung, and H. H. Liu, *Proc. R. Soc. Ser. A* **454**, 903 (1998).